AIAA JOURNAL
Vol. 35, No. 5, May 1997

Control of Vortex Pairing Sound

R. C. K. Leung* and W. F. Chu†
University of Hong Kong, Hong Kong
S. K. Tang‡
Hong Kong Polytechnic University, Hong Kong
and
N. W. M. Ko§
University of Hong Kong, Hong Kong

A study of the control of pairing sound of two identical thin vortex rings by means of a thin control vortex ring of opposite circulation is reported. Amplification and attenuation of the pairing sound have been observed. The amplification and attenuation are due to the effect of the control vortex ring on the interaction of the two pairing rings. Four basic types of interaction of the three interacting vortex rings and different degrees of amplification and attenuation have also been established.

Nomenclature

A, α	= constants depending on core vorticity distribution
c_0	= ambient speed of sound
d	= nozzle diameter of circular jet
$\boldsymbol{e}_\phi, \boldsymbol{e}_z$	= azimuthal and streamwise unit vectors, respectively
$\boldsymbol{n}$	= unit vector normal in the direction of vortex ring propagation
$p, p'_{\max}, p'_{\rm rms}$	= far-field, maximum, and root mean square pressures, respectively
$p'_{2,\max}, p'_{2,\rm rms}$	= maximum and root mean square far-field pressures, respectively, two vortex ring system
R	= initial vortex ring radius
r	= radial distance from origin
Sr_d, Sr_θ	= Strouhal numbers based on jet nozzle diameter and jet shear layer momentum thickness, respectively
ΔSPL	= sound pressure level difference
s	= element arc length on the vortex ring
t	= time
$\boldsymbol{U}_I$	= induced velocity on vortex ring
$\boldsymbol{U}_T$	= self-induced translational velocity of an isolated vortex ring
$\boldsymbol{u}$	= velocity
u_r, u_z	= radial and streamwise components of velocity, respectively
$\boldsymbol{V}$	= total propagation velocity of a vortex ring, $\boldsymbol{U}_T + \boldsymbol{U}_I$
V_r, V_z	= radial and streamwise components of vortex ring propagation velocity, respectively
$\boldsymbol{x}, \hat{\boldsymbol{x}}$	= far-field displacement and its unit vector
$\boldsymbol{y}$	= near-field displacement
z	= streamwise distance from origin
Γ	= vortex ring circulation
θ	= jet shear layer momentum thickness
λ_c	= initial separation between control and trailing vortex rings
λ_T	= initial separation between leading and trailing vortex rings
ξ	= angle between far-field displacement and common axis of vortex rings
ρ_0	= density of ambient fluid
σ	= effective vortex ring core radius
ϕ	= azimuthal angle
$\boldsymbol{\Psi}$	= velocity vector potential
ψ	= stream function
ω	= vorticity
$æ_r, æ_z$	= radial and streamwise components of vortex ring acceleration, respectively

Subscripts

c	= control vortex ring
i, j	= indices
L	= leading vortex ring
T	= trailing vortex ring

Received May 18, 1996; revision received Jan. 2, 1997; accepted for publication Jan. 17, 1997. Copyright © 1997 by the American Institute of Aeronautics and Astronautics, Inc. All rights reserved.

*Research Student, Department of Mechanical Engineering. Member AIAA.
†Student, Department of Mechanical Engineering.
‡Assistant Professor, Department of Building Services Engineering.
§Professor, Department of Mechanical Engineering.

Introduction

MODIFICATION of coherent structure development and, thus, the sound generation in the far field is of growing importance to manage and control free shear flows. Detailed discussions of this topic are presented in Ref. 1. Simply, the control of turbulence by the manipulation of coherent structures may be carried out either actively or passively. Active control, typically achieved by using acoustic excitation at the appropriate frequencies near the nozzle exit, may enhance and localize the interaction of coherent structures, causing turbulence enhancement, or may hinder the interaction, resulting in their earlier breakdown and leading to turbulence suppression. The strongest effect of periodic excitation is in the region where the forcing frequency is equal to the natural frequency of the unexcited flow. In the near field of the jet, the shear layer mode[2,3] and the preferred mode[4,5] dominate the flow. The preferred mode is characterized by a Strouhal number based on the jet diameter d of $0.25 \leq Sr_d \leq 0.5$ and is the characteristic instability frequency at the end of the potential core where the mixing layers merge. The shear layer mode is of higher frequency and is characterized by a Strouhal number Sr_θ, which is based on the momentum thickness θ. It is associated with the most amplified wave of the initial velocity profile near the nozzle. The shear layer mode of stable pairing at the excitation Sr_θ of about 0.012 results in the initial roll up and subsequent pairing of the vortical structures being accentuated.[2] The excitation of the laminar shear layer at $Sr_\theta = 0.017$ produces attenuation of turbulence intensities and of aerodynamic noise generation.[6] This is known as the suppression mode.[6] At low jet velocities, the preferred Strouhal number Sr_d is approximately proportional to the Strouhal number Sr_θ of the shear layer mode.[3,7] For higher jet velocities, the Sr_d remains constant at 0.44. The change of scaling behavior occurs at $d/2\theta = 120$ (Ref. 3).

Passive control of axisymmetric jet flow by modification of the developing coherent structures, by altering the upstream condition of the flow, is as successful as active control. The change in the initial conditions of the nozzle boundary layer[8,9] and the introduction of a concentric annular jet, forming a coaxial jet,[10–12] results in different evolutions and interactions of the coherent structures and results in significant suppression of the far-field sound generation. The latter approach has been successfully applied to jet engine noise suppression. Investigations of the flow dynamics of unexcited and excited coaxial jets of different mean velocity ratios indicate the complicated interactions of the different types of vortical structures and their dependence on the mean velocity ratios.[13–17]

In jet flow, pairings of vortex rings are found as the major activities that form the coherent structures and have been proposed as the sound source in an initially laminar air jet.[18–21] The results of theoretical and experimental investigations[18–21] suggest the relationship of the jet noise and the vortex pairing process. However, the basic sound generation mechanism in the vortex pairing process is not clearly established.

In the recent study of Tang and Ko,[22] a simple theoretical model for the sound emission from the pairing of two thin and planar vortex rings propagating on the same axis suggests that maximum sound power is radiated at the instant when the slip through process occurs. This is also the instant at which the vortex rings are highly accelerating or decelerating. The dependence of sound radiation on the acceleration or deceleration of the vortex rings is confirmed by the experimental results in an excited circular air jet.[22]

Based on the method of contour dynamics, a more recent study[23] investigated the sound generation due to the interaction between two inviscid coaxial vortex rings moving along a common axis in the same direction. The vortex ring interactions studied are found in axisymmetric jets of low Mach number. The radial accelerations and the rate of change of the axial accelerations of the vorticity centroids of the vortex rings are found to be important in the generation of sound during the interaction.

The recent study of Leung et al.[24] proposed a simplified vortex pairing noise model to account for jet noise generation. This model of mutual slip through vortex rings takes into account the formation process of the vortex rings and their subsequent pairing motions. For low Mach number jet noise, the model illustrates the eighth power law of Lighthill.[25] The amplitude of sound is found to increase linearly with nozzle diameter, which is again consistent with existing jet sound theories at 90-deg emission angle or at low Mach number.

These studies[22–24] of the vortex pairing sound concern only the interactions of two vortex rings moving along a common axis in the same direction. The effect of an additional vortex ring on their interactions and the sound generated is still not addressed. Thus, based on a simplified axisymmetric vortex model, this study is aimed at understanding the interactions of three coaxial vortex rings and their effect on the far-field sound. The additional or control vortex ring has circulation opposite to those of the other two identical rings. This simulates coaxial jets with an inverted mean velocity profile.

Model for Coaxial Vortices and Pairing Sound

Vortex pairing in the present investigation refers to the interaction of two thin identical inviscid coaxial vortex rings moving along a common axis in the same direction[24] and an additional control vortex ring with varying properties (see Fig. 1). The pairing of the two identical vortex rings with mutual slip through motion is used as the basis for comparison.

Figure 1 shows the vortex system under consideration. Because the features of the two identical coaxial vortex rings have been described in detail,[22,24] only the important features are shown in the following sections.

For inviscid axisymmetric flow without swirl of constant density, the vorticity equation in cylindrical coordinates (r, ϕ, z) (Ref. 26) is

$$\frac{\partial \omega}{\partial t} + (\boldsymbol{u} \cdot \nabla)\omega = (\omega \cdot \nabla)\boldsymbol{u} \tag{1}$$

$$\omega = -\nabla^2 \Psi \tag{2}$$

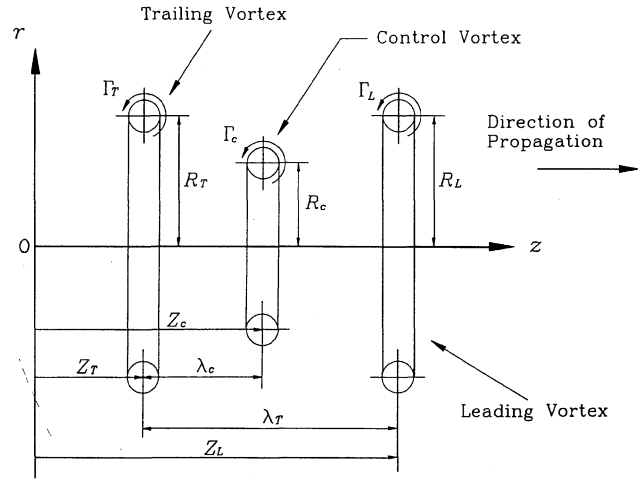

Fig. 1 Schematic diagram of vortex rings.

where $\omega = \omega \boldsymbol{e}_\phi$. The velocity is related to the vector potential as $\boldsymbol{u} = \nabla \times \Psi$ and $\Psi = (\psi/r)\boldsymbol{e}_\phi$. The velocity components in the radial and streamwise directions may be represented as

$$u_r = -\frac{1}{r}\frac{\partial \psi}{\partial z}, \qquad u_z = \frac{1}{r}\frac{\partial \psi}{\partial r} \tag{3}$$

and, hence, the azimuthal component of vorticity is

$$\omega = \frac{\partial u_r}{\partial z} - \frac{\partial u_z}{\partial r} = -\frac{1}{r}\frac{\partial^2 \psi}{\partial z^2} - \frac{\partial}{\partial r}\left(\frac{1}{r}\frac{\partial \psi}{\partial r}\right) \tag{4}$$

The motion of the multiple vortex ring system is numerically simulated, using the vortex filament model.[27] Because the motion of the vortices is purely axisymmetrical, azimuthal change is neglected in the formulation of the vortex filament model. The vortex ring velocity $\boldsymbol{V}_i$ is composed of its self-induced translational velocity $\boldsymbol{U}_{T,i}$ and the velocity $\boldsymbol{U}_{I,i}$ induced by other vortex rings, where $i = 1, 2, 3$ for the present system of three vortex rings. In the absence of external influence, the translational velocity $\boldsymbol{U}_{T,i}$ of the ith vortex ring with circulation Γ_i is given by[26]

$$\boldsymbol{U}_{T,i} = (\Gamma_i/4\pi R_i)\left[\log(8R_i/\sigma_i) - \tfrac{1}{2} + A\right]\boldsymbol{e}_z \tag{5}$$

where $\boldsymbol{e}_z$ is an unit vector in the streamwise direction, R_i the vortex ring radius, and σ_i the effective core radius at that particular instant. For vortex core with uniform vorticity distribution, $A = \frac{1}{4}$ (Ref. 26).

The induced velocity $\boldsymbol{U}_{I,i}$ on the ith vortex ring at $\boldsymbol{y}_i$ induced by other vortex rings j at $\boldsymbol{y}_j$ is expressed by the Biot–Savart law[26]:

$$\boldsymbol{U}_{I,i}(\boldsymbol{y}_i) = -\frac{1}{4\pi}\sum_{i \neq j}\int \Gamma_j \frac{\boldsymbol{y}_i - \boldsymbol{y}_j}{|\boldsymbol{y}_i - \boldsymbol{y}_j|^3} \times \frac{\mathrm{d}\boldsymbol{y}_j}{\mathrm{d}s_j}\,\mathrm{d}s_j \tag{6}$$

where Γ_j is the circulation, $\boldsymbol{y}_j$ is a position vector of fluid particle on the jth vortex ring, and $\mathrm{d}s_j$ is elemental arc length. The integrand of Eq. (6) becomes singular as $\boldsymbol{y}_i$ approaches $\boldsymbol{y}_j$ because the velocity of a vortex filament of nonvanishing curvature is infinite. Such singularity is removed by means of Rosenhead–Moore approximation[28] and the modified Biot–Savart velocity takes the form, with $\alpha = \exp(-1 - 2A)$,

$$\boldsymbol{U}_{I,i}(\boldsymbol{y}_i) = -\frac{1}{4\pi}\sum_{i \neq j}\int \Gamma_j \frac{\boldsymbol{y}_i - \boldsymbol{y}_j}{\left(|\boldsymbol{y}_i - \boldsymbol{y}_j|^2 + \alpha\sigma_j^2\right)^{\frac{3}{2}}} \times \frac{\mathrm{d}\boldsymbol{y}_j}{\mathrm{d}s_j}\,\mathrm{d}s_j \tag{7}$$

The vortex core radius σ_j may vary with time. In addition, it may be argued that σ_j should vary along the vortex ring because of different vortex stretching rates along the vortex ring. However, Moore and Saffman[29] have shown that such variations in σ_j quickly produce axial flows to redistribute the vortex volume. The time scale of redistribution is much smaller than that needed by the vortex ring to move significantly, and the redistribution can be thought of as almost

instantaneous. These considerations prompt the conservation of total volume of the vortex, that is,

$$\frac{\partial}{\partial t}\left(R_j\sigma_j^2\right) = 0 \tag{8}$$

Therefore, the position $\boldsymbol{y}_i(z_i, r_i)$ of the ith vortex ring can be obtained by integrating the following equation:

$$\boldsymbol{V}_i = \frac{\Gamma_i}{4\pi R_i}\left[\log\left(\frac{8R_i}{\sigma_i}\right) - \frac{1}{2} + A\right]\boldsymbol{e}_z - \frac{1}{4\pi}\sum_{i\neq j}\int \Gamma_j \frac{\boldsymbol{y}_i - \boldsymbol{y}_j}{\left(|\boldsymbol{y}_i - \boldsymbol{y}_j|^2 + \alpha\sigma_j^2\right)^{\frac{3}{2}}} \times \frac{\mathrm{d}\boldsymbol{y}_j}{\mathrm{d}s_j}\,\mathrm{d}s_j \tag{9}$$

with respect to time, using the fourth-order Runge–Kutta method. The velocity V_i and acceleration $æ_i$ of the ith vortex ring are calculated by differentiating its position with respect to time:

$$V_i = (V_{z,i}, V_{r,i}) = \frac{\mathrm{d}}{\mathrm{d}t}(z_i, r_i) \tag{10}$$

and

$$æ_i = (æ_{z,i}, æ_{r,i}) = \frac{\mathrm{d}^2}{\mathrm{d}t^2}(z_i, r_i) \tag{11}$$

The far-field wave equation for low Mach number flow is

$$\nabla^2 p - \frac{1}{c_0^2}\frac{\partial^2 p}{\partial t} = -\rho_0 \nabla \cdot (\boldsymbol{\omega} \times \boldsymbol{u})$$

where p, c_0, and ρ_0 denote the far-field pressure, the ambient speed of sound, and the density of the medium, respectively.[30] For a system of thin vortex rings moving along a common axis parallel to unit vector $\boldsymbol{n}$, the far-field sound pressure fluctuations $p(\boldsymbol{x}, t)$ at a distance $\boldsymbol{x}$ in the far field are of the form[19]

$$p(\boldsymbol{x}, t) = \frac{\rho_0}{4c_0^2|\boldsymbol{x}|^3}\left[\boldsymbol{x}\cdot\left(\boldsymbol{nn} - \frac{1}{3}\right)\cdot\boldsymbol{x}\right]\frac{\mathrm{d}^3 Q}{\mathrm{d}t^3} = \frac{\rho_0}{4c_0^2|\boldsymbol{x}|}\left(\cos^2\xi - \frac{1}{3}\right)\frac{\mathrm{d}^3 Q}{\mathrm{d}t^3} \tag{12}$$

where

$$Q = \sum_i \Gamma_i R_i^2 z_i$$

where ξ is the angle between the far-field point and the common axis with $\cos\xi = \hat{\boldsymbol{x}}\cdot\boldsymbol{n}$. The amplitude of the far-field sound pressure fluctuations depends on the properties of the vortices, and the directivity of the far field is quadrupole in nature, as revealed in the bracketed terms in Eq. (12).

The normalized time and velocity are $t' = t/(R_T^2/\Gamma_T)$ and $v' = v/(\Gamma_T/R_T)$. The length of reference is taken to be R_T, and the normalized pressure is $p' = p/(\Gamma_T^2/R_T^2)$. The regime of study covers $0.4 \le R_c/R_T \le 2.0$ and $-2.0 \le \Gamma_c/\Gamma_T \le -0.01$ and the separation ratio λ_c/λ_T of 0, 0.25, 0.5, 0.75, and 1, where $\lambda_c = (z_c - z_T)$ and $\lambda_T = (z_L - z_T) = R_T$, which is the gap of the two identical vortex rings. The core-to-ring-radius ratios of the three vortex rings are 0.1. The computation was carried out at $0 \le t' \le 50$. The spatial integration along the periphery of the vortex ring is done by Simpson's method[31] with 360 segments. The normalized time step used in computation is $\Delta t' = 0.02$. Several smaller values of $\Delta t'$ and more spatial segments for each vortex ring have been attempted but no observable change can be found.

Results and Discussion

Because the characteristics of the two vortex ring system will be used for comparison, the time distribution of the normalized far-field pressure p' of repetitive pairings or slip throughs has been computed. The maximum $p'_{2,\max}$ within the time span of $0 \le t' \le 50$ is 0.715, and its root mean square sound pressure $p'_{2,\mathrm{rms}}$ is 0.21. As shown experimentally by Tang and Ko,[22] for the pairing of the two thin vortex rings, the maximum sound pressure is radiated at the instant of the occurrence of the slip through process at which high acceleration or deceleration of the two vortices are found. The normalized axial and radial accelerations of the two interacting vortex rings have also been determined. It is found that, during the slip through, the trailing vortex ring accelerates, while the leading one decelerates. The acceleration is significantly higher than the deceleration. Their roles change during the next slip through. For the interaction of the thin core vortex rings, the radial components are mainly responsible for the far-field sound pressure fluctuations.[22]

With the introduction of the third control vortex ring of opposite circulation, the far-field sound pressures, both the maximum $p'_{\max}$ and root mean square sound pressure p'_{rms}, have been computed. The root mean square sound pressure p'_{rms} is adopted for presentation as it is related to the sound power explicitly if the sound source is steady or within a short time interval. The attenuation and amplification of sound pressure level $\Delta\mathrm{SPL} = 10\log_{10}(p'^2_{\mathrm{rms}}/p'^2_{2,\mathrm{rms}})$ in decibels, due to the presence of the control vortex ring, in comparison with that of two rings, at the separation ratios $\lambda_c/\lambda_T = 0, 0.25, 0.5, 0.75,$ and 1 are shown in Figs. 2a–2e, respectively. For $\lambda_c/\lambda_T = 0$ and 1, as the core-to-ring-radius ratio of the vortex rings is 0.1, the results at which two vortex rings overlap are not presented. For the isocontours, the solid lines indicate attenuation of sound pressure due to the presence of the control vortex ring and the dotted lines indicate amplification. Generally, Figs. 2a–2e show that attenuation ΔSPL of the sound pressure is found at ring-radius ratio $R_c/R_T > 1$ and in the first and in half of the second quadrants. In the third and fourth quadrants amplification is mainly found. For $R_c/R_T < 1$, there is also a small region of minor attenuation at circulation ratio $\Gamma_c/\Gamma_T \approx -1$ (Figs. 2b and 2c). In addition, in Fig. 2 the maximum amplification is about +55 dB at the separation ratios $\lambda_c/\lambda_T = 0, 0.5,$ and 1.0. For $\lambda_c/\lambda_T = 0$ and 1, the positions of maximum amplification are nearly the same, at $R_c/R_T \approx 1.25$ and $\Gamma_c/\Gamma_T \approx -1.8$ of the second quadrant (Figs. 2b and 2e). For $\lambda_c/\lambda_T = 0.5$, the position of maximum amplification is at $R_c/R_T \approx 0.6$ and $\Gamma_c/\Gamma_T \approx -0.8$ of the fourth quadrant. It is also in this quadrant that strongest amplification is found for the other two vortex separation ratios of $\lambda_c/\lambda_T = 0.25$ and 0.75 (Figs. 2b and 2d). This phenomenon suggests that the phase of the control vortex ring with respect to the other two rings is also an important parameter.

The maximum attenuation of the far-field sound pressure is about −19 dB at $\lambda_c/\lambda_T = 0.5$ (Fig. 2c). For other separation ratios, the maximum attenuation is only about −16 dB. These maximum attenuations are significantly lower than those of amplification of about +55 dB. The positions of the maximum attenuation are mainly in the second quadrant. The regime where attenuation occurs generally shrinks from the biggest at $\lambda_c/\lambda_T = 0$ (Fig. 2a) to the smallest at $\lambda_c/\lambda_T = 1$ (Fig. 2e). As amplification, the phase of the control vortex ring is also important.

Thus, these phenomena indicate that attenuation is mainly achieved as the control vortex ring has ring radius greater than those of the other two rings and its circulation is in opposite direction of rotation. For the control vortex ring circulation greater than those of the two vortex rings $|-\Gamma_c/\Gamma_T| > 1$, attenuation is only achieved at higher radius ratios, while amplification is found at lower radius ratios. For smaller control vortex ring of $R_c/R_T < 1$, minor attenuation is achieved at $\Gamma_c/\Gamma_T \approx -1$. The phase of the control vortex ring with respect to the other two rings does not affect the attenuation too significantly rather, the extent of the regime where attenuation can be achieved is affected.

These isocontours indicate the effect of the control vortex ring on the far-field sound. To understand the mechanism causing the attenuation or amplification, the dynamics of the three vortex rings during their interaction are desirable. Although the positions, velocities, and accelerations of the three interacting vortex rings at all of the conditions shown in Fig. 2 have been computed, only the representative ones will be presented in the following sections. Inasmuch as the isocontours of Fig. 2 indicate local peaks of intense and moderate amplification and similarly for attenuation, though to lesser extent, four representative cases of amplification and attenuation are presented. For amplification, they are marked as intense amplification (IA) ($\lambda_c/\lambda_T = 0.5$, $R_c/R_T = 0.6$, and $\Gamma_c/\Gamma_T = -0.8$) and moderate amplification (MA) ($\lambda_c/\lambda_T = 0.5$, $R_c/R_T = 0.8$, and $\Gamma_c/\Gamma_T = -1$) and as moderate attenuation (MR) ($\lambda_c/\lambda_T = 0.75$, $R_c/R_T = 1.8$, and $\Gamma_c/\Gamma_T = -1.2$) and small attenuation (SR) ($\lambda_c/\lambda_T = 0.25$,

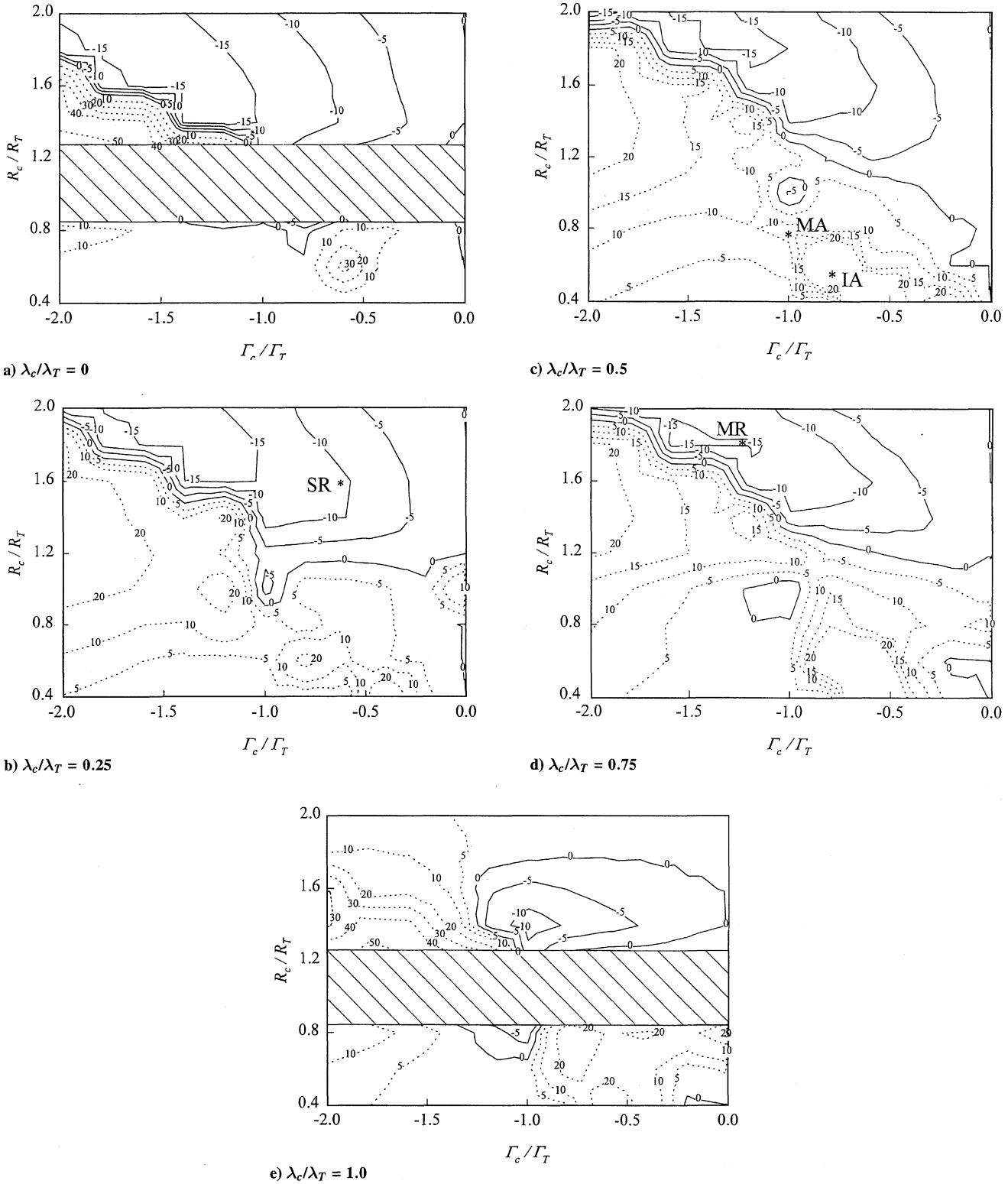

Fig. 2 Isocontours of difference of far-field sound pressure: ——, attenuation; and · · · · ·, amplification; crosshatch regions are where vortex cores overlap; plus or minus decibels.

$R_c/R_T = 1.6$, and $\Gamma_c/\Gamma_T = -0.6$) (Fig. 2b–2d). For the former two, the respective amplifications are about +55 and +10 dB. For the latter two, the attenuations are about −15 and −10 dB, respectively. As will be shown later, they represent four basic types of sound generation due to the vortex interaction.

For the local peak of IA, the nondimensional far-field sound pressure p' with nondimensional time t' at $\lambda_c/\lambda_T = 0.5$, $R_c/R_T = 0.6$, and $\Gamma_c/\Gamma_T = -0.8$ is shown in Fig. 3. Within the time $0 \leq t' \leq 50$, there are peaks of extremely high pressure within the short time span of $11 < t' < 12$. At other times, no significant pressure peak is found. The peak pressures are as high as +3000 and as low as −7550. These peak levels compare with +0.719 and −0.184 of the two vortex ring system, suggesting the presence of the control vortex ring results in very intense and transient far-field sound pressure radiation.

The paths of the three vortex rings at IA are shown in Fig. 4, in which intense interaction of the control vortex ring with both the initially leading and initially trailing vortex rings occurs within the short time span of $11 < t' < 12$. During this period, there are very rapid interactions of the three vortex rings within a very small area.

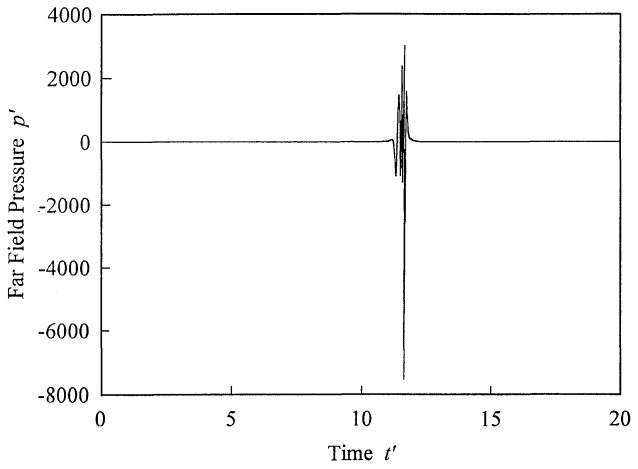

Fig. 3 Far-field sound pressure at intense amplification; control vortex ring: $\lambda_c/\lambda_T = 0.5$, $R_c/R_T = 0.6$, and $\Gamma_c/\Gamma_T = -0.8$.

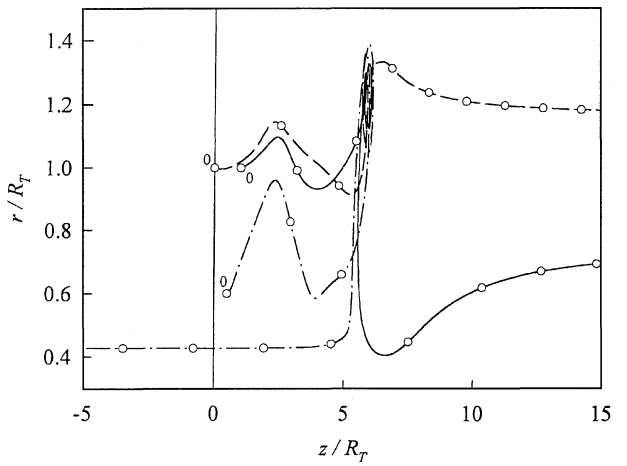

Fig. 4 Locations of three interacting vortex rings at IA with control vortex ring: $\lambda_c/\lambda_T = 0.5$, $R_c/R_T = 0.6$, and $\Gamma_c/\Gamma_T = -0.8$. ——, leading vortex ring; – – –, trailing vortex ring; and – · –, control vortex ring.

After this intense interaction, Fig. 4 shows that the control vortex ring moves upstream, in the opposite direction of those of the other two vortex rings. Further, after this intense interaction the separation of the other two vortex rings is so large that no further interaction and slip through is found.

The streamwise and radial accelerations of the three vortex rings at IA are shown in Figs. 5a and 5b. The accelerations or decelerations of both components of the three vortex rings are of the same order of magnitudes of about ±50, implying that these three vortex rings change their roles, and correspondingly their accelerations, during the very rapid interactions. These accelerations are much higher than those of two vortex ring system of about ±0.3, indicating their very intense interactions due to the presence of the control vortex ring.

In the MA regime at $\lambda_c/\lambda_T = 0.5$, $R_c/R_T = 0.8$, and $\Gamma_c/\Gamma_T = -1$, the amplification is about +10 dB. The corresponding time variation of the far-field sound pressure p' is shown in Fig. 6. The maximum and minimum pressures of the two vortex ring system are also shown for comparison. In this regime, Fig. 6 shows that the presence of the control vortex results in less change in the magnitude of the far-field sound pressure than that of two vortex ring system at $t' < 6$. During this period, the control vortex ring interacts with both the initially leading and the trailing vortex rings at $z' < 2$ ($t' < 4$), before it convects upstream, away from the other two vortex rings, and loses its influence (Fig. 7). At $z' > 2(t' > 4)$ the other two vortex rings adjust themselves and then repetitive slip throughs occur. These slip throughs, and thus, the far-field sound pressure (Fig. 6), have higher magnitude (+2.4 and −0.6) and higher frequency components than those of the two vortex ring system.

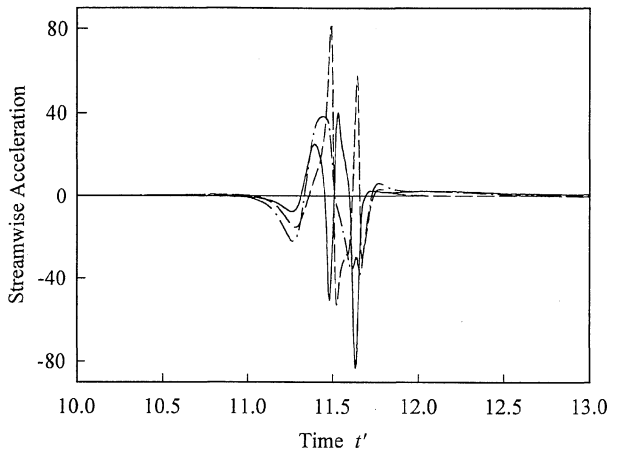

a) Streamwise acceleration

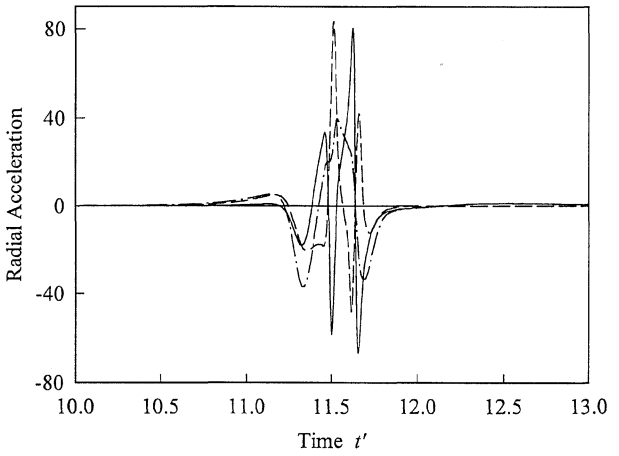

b) Radial acceleration

Fig. 5 Time variations of accelerations of vortex rings at IA with control vortex ring: $\lambda_c/\lambda_T = 0.5$, $R_c/R_T = 0.6$, and $\Gamma_c/\Gamma_T = -0.8$. ——, leading vortex ring; – – – trailing vortex ring; and – · –, control vortex ring.

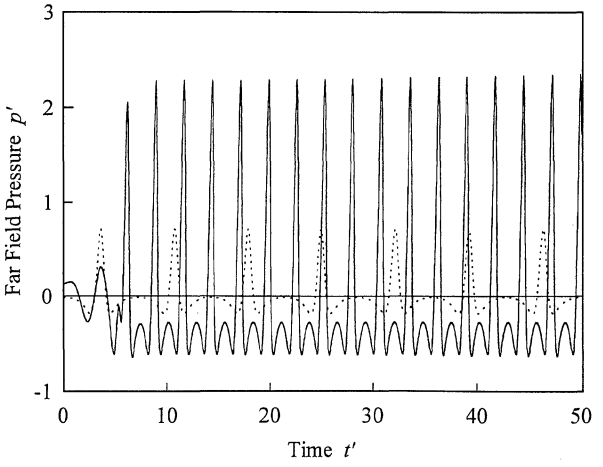

Fig. 6 Far-field sound pressure at MA with control vortex ring: $\lambda_c/\lambda_T = 0.5$, $R_c/R_T = 0.8$, and $\Gamma_c/\Gamma_T = -1.0$. · · · · ·, two vortex ring system.

The streamwise and radial accelerations of the three vortex rings are shown in Figs. 8a and 8b, respectively. At $t' < 4$ ($z' < 2$), the lower radial decelerations of the control and initially trailing vortex rings, which are in phase, seem to be responsible for the slight change in the magnitude of the sound pressure (Fig. 6). During the repetitive slip throughs, both components of accelerations of the initially leading and trailing vortex rings are higher than those of the two vortex system. Further, the radial accelerations and decelerations of

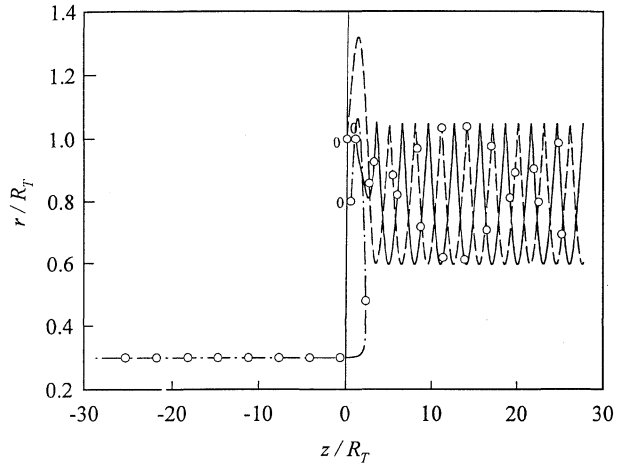

Fig. 7 Locations of three interacting vortex rings at MA with control vortex ring: $\lambda_c/\lambda_T = 0.5$, $R_c/R_T = 0.8$, and $\Gamma_c/\Gamma_T = -1.0$. ——, leading vortex ring; – – –, trailing vortex ring; and – · –, control vortex ring.

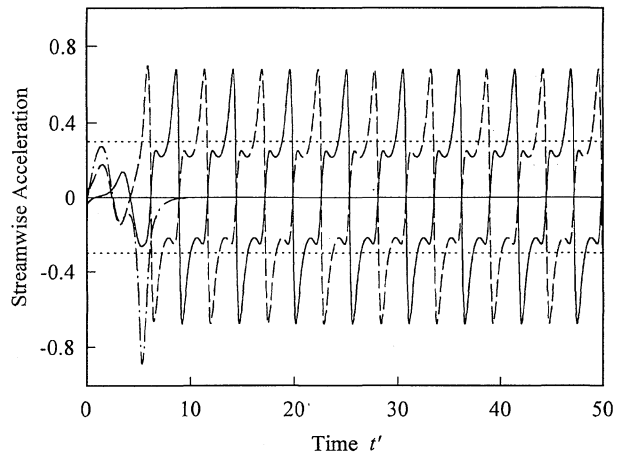

a) Streamwise acceleration

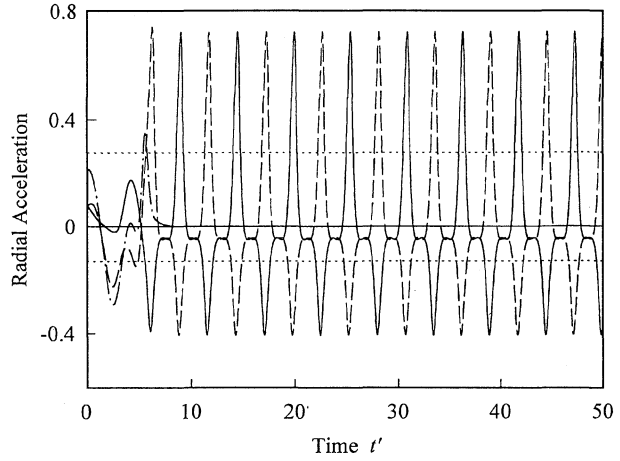

b) Radial acceleration

Fig. 8 Time variations of accelerations of vortex rings at MA with control vortex ring: $\lambda_c/\lambda_T = 0.5$, $R_c/R_T = 0.8$, and $\Gamma_c/\Gamma_T = -1.0$. ——, leading vortex ring; – – –, trailing vortex ring; – · –, control vortex ring; and · · · · ·, limits of two vortex ring system.

the two interacting vortex rings also are responsible for the sound generated (Figs. 6 and 8b).

At SR of -10 dB ($\lambda_c/\lambda_T = 0.25$, $R_c/R_T = 1.6$, and $\Gamma_c/\Gamma_T = -0.6$) the time variation of the sound pressure, as shown in Fig. 9, indicates lower pressure magnitude both in the time span when the effect of the control vortex ring is still present, $t' < 5$, and in the subsequent time span when repetitive slip throughs are found. For the latter, lower frequency components than those of two vortex system

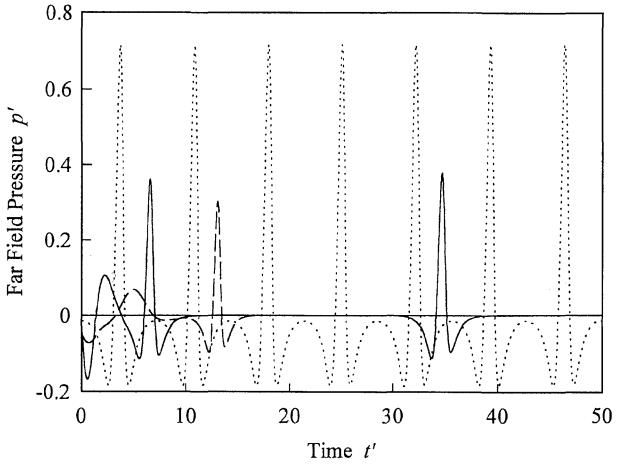

Fig. 9 Far-field sound pressures at SR and MR with control vortex ring. – – –, SR: $\lambda_c/\lambda_T = 0.25$, $R_c/R_T = 1.6$, and $\Gamma_c/\Gamma_T = -0.6$; ——, MR: $\lambda_c/\lambda_T = 0.75$, $R_c/R_T = 1.8$, and $\Gamma_c/\Gamma_T = -1.2$; and · · · · ·, two vortex ring system.

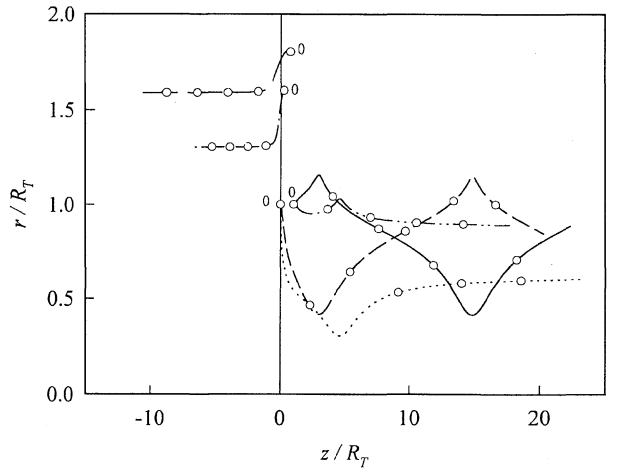

Fig. 10 Locations of three interacting vortex rings at SR and MR with control vortex ring where for SR $\lambda_c/\lambda_T = 0.25$, $R_c/R_T = 1.6$, and $\Gamma_c/\Gamma_T = -0.6$: ——, leading vortex ring; – – –, trailing vortex ring; and – · –, control vortex ring and where for MR $\lambda_c/\lambda_T = 0.75$, $R_c/R_T = 1.8$, and $\Gamma_c/\Gamma_T = -1.2$: – · · –, leading vortex ring; · · · · ·, trailing vortex ring; and – – –, control vortex ring.

are found. The control vortex ring at $R_c/R_T = 1.6$ convects toward the two vortex rings while it moves upstream (Fig. 10). This results in lower streamwise and radial accelerations of the initially leading and trailing vortex rings at $t' < 5$ and lower radial accelerations of both rings at $t' > 5$ (Fig. 11), suggesting the control vortex ring suppresses their interaction, and thus, the sound is generated.

At MR of -15 dB ($\lambda_c/\lambda_T = 0.75$, $R_c/R_T = 1.8$, and $\Gamma_c/\Gamma_T = -1.2$), the time variation of the sound pressure is also shown in Fig. 9. The main differences of this MR from the SR are the lower pressures of the initial interactions of the three vortex rings and only one subsequent slip though (Fig. 10). The absence of other slip through of the two vortex rings and the associated acceleration (Figs. 11a and 11b) is the cause for slightly greater attenuation.

The power spectra of the far-field sound pressures of the four cases and of the two vortex ring system are shown in Fig. 12. The broad spectrum of MR does not have the discrete spectral peaks and is of lower level than that of SR. The latter has more discrete peaks but is lower than those of the two vortex ring system. The spectrum of MA has higher levels and more higher frequency components than those of the two vortex system. The spectrum of IA tends to be broad and has a significant increase in the high-frequency components.

Thus, the preceding account of the findings of three interacting thin vortex rings indicate the differences of the effect of the control vortex ring on the interaction of the two vortex rings. The four representative cases of interaction of the three vortex rings and their

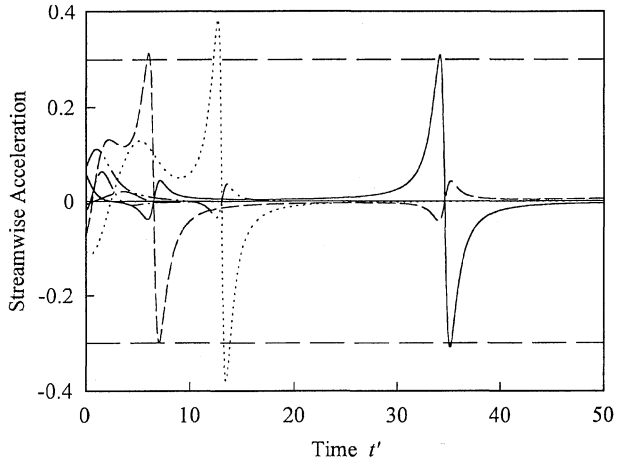

a) Streamwise acceleration

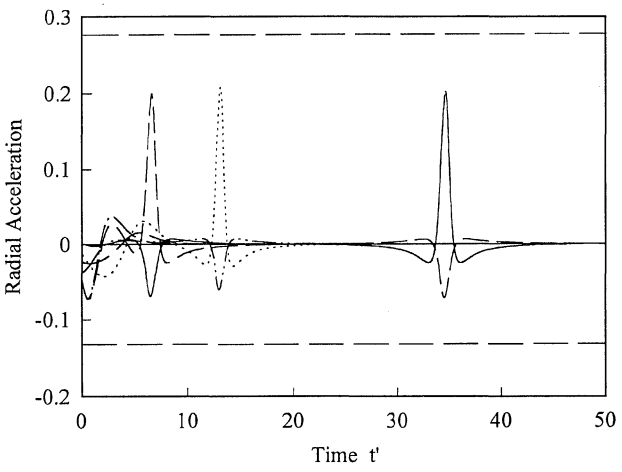

b) Radial acceleration

Fig. 11 Time variations of accelerations of vortex rings at SR and MR where symbols are as in Fig. 12; ——, limits of two vortex ring system.

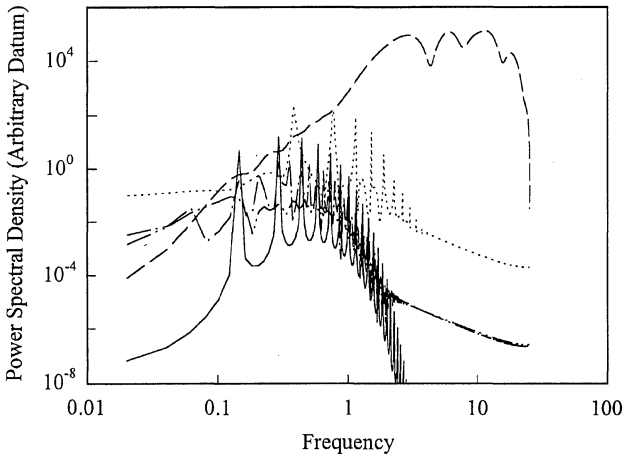

Fig. 12 Spectra of far-field sound pressure: ——, two vortex ring system; – – –, IA; · · · · ·, MA; – · –, SR; and – · · –, MA.

subsequent movement illustrate the importance of the parameters of radius ratio, circulation ratio, and their phase. Amplification and attenuation of the far-field sound depends mainly on these parameters and on the accelerations of the three vortex rings. A 10-dB amplification of far-field sound pressure and the change of vortex accelerations were observed by Tang and Ko[22] in a circular air jet under acoustic excitation. Though the amplification is nearly of the order of magnitude as the MA of the present study, no direct comparison can be made because the circular jet was controlled by

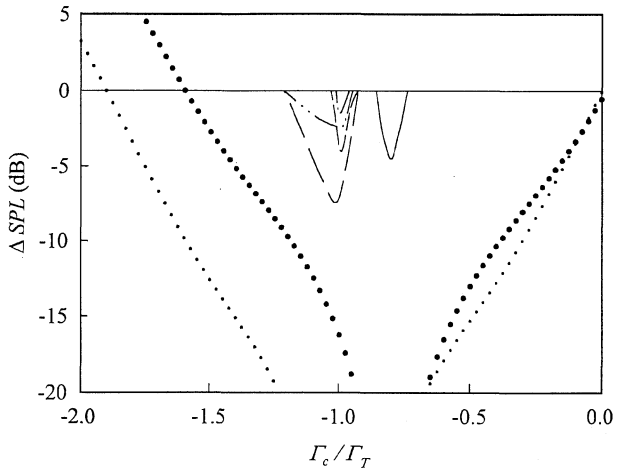

Fig. 13 Difference in far-field sound pressures: ——, $\lambda_c/\lambda_T = 0$; – – –, $\lambda_c/\lambda_T = 0.25$; – · –, $\lambda_c/\lambda_T = 0.5$; – · · · – $\lambda_c/\lambda_T = 0.75$; — —, $\lambda_c/\lambda_T = 1.0$; and · · · · ·, $R_c/R_T = 0.95$ and • • •, $R_c/R_T = 0.8$ (Ref. 12).

active means.[22] Also, Tang and Ko[22] did not show how far-field sound pressure level would be affected by the change in vortex ring acceleration or deceleration.

Because there is lack of experimental data on the far-field sound pressure of two and three interacting vortex ring systems for comparison with the present study, the available results of coaxial jets are used to evaluate the present findings. The present cases of $R_c/R_T < 1$ and $\lambda_c/\lambda_T < 1$ are similar to the inverted velocity profile coaxial jets.[12] However, in the initial region of coaxial jets, the two potential cores of mean jet exit velocities would affect the interaction of the inner and outer jet vortex trains. It is only in the intermediate zone that the two trains of coherent structures, of bigger sizes and in more diffused state, interact. However, in the intermediate zone, the mean shear is also present, and one would expect it would affect their mutual induction and interaction. Further, in coaxial jets of mean velocity ratio (inner to outer) of less than unity, in the beginning of the intermediate zone, the initial inner and outer jet vortices have evolved and interacted, resulting in complicated form of interaction. The present assumption of thin core vortex ring is not really valid. Tanna[11] reported an attenuation of 8 dB in the low-frequency region and an amplification of 9 dB in the high-frequency region of a coaxial jet of inverted velocity profile. Their orders of magnitude are similar to those of the MA (+10 dB) and SR (−10 dB) regimes. However, because the circulations of the two vortex trains in the initial region, the relative vortex separation λ_c/λ_T, and the location of control vortex ring cannot be explicitly determined from the experiment, comparison between the results from the experiment and present study is not feasible. Nevertheless, based on the model of vortex pairing for jet noise generation, the circulation of the shear layer jet vortices is then related to the jet exit velocity,[24] and the attenuations of far-field sound ΔSPL at $R_c/R_T < 1$ of the present study are plotted in Fig. 13. The experimental results in the intermediate zone of coaxial jets of inverted velocity profile with Mach number 0.5–2.0 are also shown.[12] Despite the difference in the magnitude and the aforementioned differences between the present assumption of thin vortex rings with the coherent structures of coaxial jets, basically, a similar trend for these two sets of data is found.

Conclusions

This paper reports the use of a thin vortex ring of opposite circulation to control the pairing sound of two identical vortex rings. Based on the Biot–Savart induction law for the motions of the vortex rings and the far-field sound formula, the effect of the control vortex ring is found to depend on the radius ratio, circulation ratio, and separation of the control ring with the other two rings.

With the introduction of the control vortex ring, amplification and attenuation of the pairing sound of the two vortex rings have been found. Attenuation of the pairing sound is mainly achieved because the control vortex ring has radius greater than those of the pairing vortex rings and of circulation ratio $-1 \leq \Gamma_c/\Gamma_T < 0$. For lower

circulation of the control vortex ring than those of the pairing vortex rings ($\Gamma_c/\Gamma_T < -1$), the radius of the control vortex would have to be bigger before attenuation can be achieved.

In the present system, due to the introduction of the control vortex ring, higher amplification than attenuation of the pairing sound is observed. There are four basic types of interaction, resulting in different degrees of amplification and attenuation. The IA is due to the much more rigorous interaction and the significant increase in the acceleration and deceleration of the three interacting vortices. The MA is the result of initial minor interaction with the control vortex ring and the slightly enhanced pairing of the initially leading and trailing vortices. For attenuation, the SR involves the minor interaction and slight suppression of the pairing of the two pairing vortex rings by the control vortex ring. However, subsequent repetitive slip throughs, their acceleration and deceleration, and the associated far-field pressure are still found. For MR, the control vortex ring suppresses the initial interaction and the subsequent slip through, resulting in lower acceleration and far-field sound.

References

[1]Fiedler, H. E., and Fernholz, H. H., "On Management and Control of Turbulent Shear Flows," *Progress in Aerospace Science*, Vol. 27, 1990, pp. 305–387.

[2]Zaman, K. B. M. Q., and Hussain, A. K. M. F., "Turbulence Suppression in Free Shear Flows by Controlled Excitation," *Journal of Fluid Mechanics*, Vol. 103, 1981, pp. 133–159.

[3]Ho, C. M., and Huerre, P., "Perturbed Free Shear Layers," *Annual Review of Fluid Mechanics*, Vol. 16, 1984, pp. 365–424.

[4]Crow, S. C., and Champagne, F. H., "Orderly Structure in Jet Turbulence," *Journal of Fluid Mechanics*, Vol. 48, Pt. 3, 1971, pp. 547–591.

[5]Gutmark, E., and Ho, C. M., "Preferred Modes and the Spreading Rates of Jets," *Physics of Fluids*, Vol. 26, No. 10, 1983, pp. 2932–2938.

[6]Hussain, A. K. M. F., and Hasan, M. A. Z., "Turbulence Suppression in Free Turbulent Shear Flows Under Controlled Excitation. Part 2. Jet-Noise Reduction," *Journal of Fluid Mechanics*, Vol. 150, 1985, pp. 159–168.

[7]Kibens, V., "The Limit of Initial Shear Layer Influence on Jet Development," AIAA Paper 81-1960, 1981.

[8]Bridges, J. E., and Hussain, A. K. M. F., "Roles of Initial Conditions and Vortex Pairing in Jet Noise," *Journal of Sound and Vibration*, Vol. 117, No. 2, 1987, pp. 289–311.

[9]Zaman, K. B. M. Q., "Effect of Initial Condition on Subsonic Jet Noise," *AIAA Journal*, Vol. 23, No. 9, 1985, pp. 1370–1373.

[10]Williams, T. J., Ali, M. R. M. H., and Anderson, J. S., "Noise and Flow Characteristics of Coaxial Jets," *Journal of Mechanical Engineering Science*, Vol. 11, No. 2, 1969, pp. 133–142.

[11]Tanna, H. K., "Coannular Jets—Are They Really Quiet and Why?" *Journal of Sound and Vibration*, Vol. 72, No. 1, 1980, pp. 97–118.

[12]Kuznetsov, V. M., and Munin, A. G., "Coaxial Jet Noise and Isothermal Jets," *Soviet Physics Acoustics*, Vol. 24, No. 6, 1978, pp. 498–502.

[13]Kwan, A. S. H., and Ko, N. W. M., "Coherent Structures in Subsonic Coaxial Jets," *Journal of Sound and Vibration*, Vol. 48, No. 2, 1976, pp. 203–219.

[14]Au, H., and Ko, N. W. M., "Coaxial Jets of Different Mean Velocity Ratios. Part 2," *Journal of Sound and Vibration*, Vol. 116, No. 3, 1987, pp. 427–443.

[15]Dahm, W. J. A., Frieler, C. E., and Tryggvason, G., "Vortex Structure and Dynamics in the Near Field of a Coaxial Jet," *Journal of Fluid Mechanics*, Vol. 241, 1992, pp. 371–402.

[16]Tang, S. K., and Ko, N. W. M., "Experimental Investigation of the Structure Interaction in an Excited Coaxial Jet," *Experimental Thermal and Fluid Science*, Vol. 8, No. 3, 1994, pp. 214–229.

[17]Wicker, R. B., and Eaton, J. K., "Near Field of a Coaxial Jet With and Without Axial Excitation," *AIAA Journal*, Vol. 32, No. 3, 1994, pp. 542–546.

[18]Winant, C. D., and Browand, F. K., "Vortex Pairing: The Mechanism of Turbulent Mixing-Layer Growth at Moderate Reynolds Numbers," *Journal of Fluid Mechanics*, Vol. 63, Pt. 2, 1974, pp. 237–255.

[19]Möhring, W., "On Vortex Sound at Low Mach Number," *Journal of Fluid Mechanics*, Vol. 65, No. 4, 1978, pp. 685–691.

[20]Kibens, V., "Discrete Noise Spectrum Generated by an Acoustically Excited Jet," *AIAA Journal*, Vol. 18, No. 4, 1980, pp. 434–441.

[21]Laufer, J., and Yen, T., "Noise Generation by a Low Mach Number Jet," *Journal of Fluid Mechanics*, Vol. 134, 1983, pp. 1–31.

[22]Tang, S. K., and Ko, N. W. M., "A Study on the Noise Generation Mechanism in a Circular Jet," *Journal of Fluids Engineering*, Vol. 115, No. 3, 1993, pp. 425–435.

[23]Tang, S. K., and Ko, N. W. M., "On Sound Generated from the Interaction of Two Inviscid Coaxial Vortex Rings Moving in the Same Direction," *Journal of Sound and Vibration*, Vol. 187, No. 2, 1995, pp. 287–310.

[24]Leung, R. C. K., Tang, S. K., Ho, I. C. K., and Ko, N. W. M., "Vortex Pairing as a Model for Jet Noise Generation," *AIAA Journal*, Vol. 34, No. 4, 1996, pp. 669–677.

[25]Lighthill, M. J., "On Sound Generated Aerodynamically: II. Turbulence as a Source of Sound," *Proceedings of the Royal Society of London, Series A*, Vol. 222, 1954, pp. 1–32.

[26]Saffman, P. G., *Vortex Dynamics*, Cambridge Univ. Press, New York, 1992, pp. 192–208.

[27]Oshima, Y., Noguchi, T., and Oshima, K., "Numerical Study of Interaction of Two Vortex Rings," *Fluid Dynamics Research*, Vol. 1, 1986, pp. 215–227.

[28]Moore, D. W., "Finite Amplitude Waves on Aircraft Trailing Vortices," *Aeronautical Quarterly*, Vol. 23, 1972, pp. 307–314.

[29]Moore, D. W., and Saffman, P. G., "The Motion of a Vortex Filament with Axial Flow," *Philosophical Transactions of the Royal Society London*, Vol. A272, 1972, pp. 403–429.

[30]Powell, A., "Theory of Vortex Sound," *Journal of the Acoustical Society of America*, Vol. 36, No. 1, 1964, pp. 177–195.

[31]Evans, G., *Practical Numerical Integration*, Wiley, New York, 1993, pp. 2–9.

S. Glegg
Associate Editor